Hourly soil temperature prediction using integrated machine learning methods, GLUE uncertainty analysis, Taguchi search, and wavelet coherence analysis

Akram Seifi (a.seifi@vru.ac.ir)
Rafsanjan University of Vali Asr https://orcid.org/0000-0003-0887-1217
Mohammad Ehteram
Semnan University
Fatemeh Nayebloei
Tarbiat Modares University
Fatemeh Soroush
Rafsanjan University of Vali Asr
Bahram Gharabaghi
University of Guelph
Ali Torabi Haghighi
University of Oulu: Oulun Yliopisto

Research Article

Keywords: Bio-inspired meta-heuristic optimization, Soil depth, Sunflower optimization, Uncertainty analysis, Wavelet coherence analysis.

Posted Date: April 19th, 2021

DOI: https://doi.org/10.21203/rs.3.rs-285852/v1

Version of Record: A version of this preprint was published at Soft Computing on July 12th, 2021. See the published version at https://doi.org/10.1007/s00500-021-06009-4.

Hourly soil temperature prediction using integrated machine learning methods, GLUE uncertainty analysis, Taguchi search, and wavelet coherence analysis

Akram Seifi[1*], Mohammad Ehteram[2], Fatemeh Nayebloei[3], Fatemeh Soroush[1], Bahram Gharabaghi[4], Ali Torabi Haghighi[5]

[1]Department of Water Science & Engineering, College of Agriculture, Vali-e-Asr University of Rafsanjan, Iran.

[2]Department of Water Engineering and Hydraulic Structures, Faculty of Civil Engineering, Semnan University, Semnan, Iran.

[3]Department of Irrigation and Drainage Engineering, Tarbiat Modares University, Tehran, Iran. ([*]Corresponding author: a.seifi@vru.ac.ir) https://orcid.org/0000-0003-0887-1217

[4]Professor, School of Engineering, University of Guelph, Guelph, Ontario, NIG 2W1, Canada; bgharaba@uoguelph.ca; DOI: 0000-0003-0454-2811.

[5]Water, Energy and Environmental Engineering Research unit, University of Oulu, P.O. Box 4300, FIN-90014 Oulu, Finland.

Abstract

In this study, hourly T_s variations at 5, 10, and 30 cm soil depth were investigated and predicted for an arid site (Sirjan) and a semi-humid site (Sanandaj) in Iran. Standalone machine learning models (adaptive neuron fuzzy interface system (ANFIS), support vector machine model (SVM), radial basis function neural network (RBFNN), and multilayer perceptron (MLP)) were hybridized with four optimization algorithms (sunflower optimization (SFO), firefly algorithm (FFA), salp swarm algorithm (SSA), particle swarm optimization (PSO)) to improve prediction accuracy and reduce uncertainty. Uncertainty analysis was performed using generalized likelihood uncertainty estimation (GLUE), while wavelet coherence was used to assess interactions between T_s and

meteorological parameters. For the arid site, ANFIS-SFO (RMSE=1.18ºC, MAE=1.05ºC, NSE=0.93, PBIAS=7%, and R^2=0.9998) produced the most accurate performance at 5 cm soil depth. At best, hybridization with SFO (ANFIS-SFO, MLP-SFO, RBFNN-SFO, SVM-SFO) decreased RMSE by 5.6, 18, 18.3, and 18.18 % compared with the respective standalone model. At the semi-humid site, all integrated models showed most accurate performance at 10 cm soil depth, with RMSE for the best model (ANFIS-SFO) increasing by 10.5%, and MAE by 10.1%, from 10 to 30 cm depth. GLUE analysis confirmed that integrating optimization algorithms with machine learning models decreased the uncertainty in T_s predictions. Wavelet coherence analysis demonstrated that air temperature, relative humidity, and solar radiation, but not wind speed, had high coherence with T_s at different soil depths at both sites, and meteorological parameters mostly influenced T_s in upper soil layers.

Keywords: Bio-inspired meta-heuristic optimization, Soil depth, Sunflower optimization, Uncertainty analysis, Wavelet coherence analysis.

1- Introduction

Soil temperature (T_s) is an influential and vital parameter in sustainable agriculture and geosciences practices, since it greatly influences physical, geological, chemical, and microbiological processes in the soil (Feng et al. 2019; Alizamir et al. 2020; Singh et al. 2018). Thus, good knowledge of T_s is required for soil, plant, and water planning and management (Zeynoddin et al. 2020). Good knowledge of T_s is also essential for modeling hydrological, meteorological, environmental, and geothermal applications, building energy requirements, etc. (Bonakdari et al. 2019). Soil temperature is dependent on different conditions and parameters,

including soil properties (porosity, bulk density, grain size, chemical composition, water content), land factors (land cover, geometric and topographic characteristics), and atmospheric and meteorological factors (solar radiation, air temperature, precipitation, wind speed, pressure gradient) (Lehnert et al. 2014; Stajkowski et al. 2020).

It is difficult, costly, and time-consuming to measure hourly T_s directly (Feng et al. 2019). Therefore, T_s measurements are not easily available for developing countries, such as Iran (Mehdizadeh et al. 2020a). In addition, T_s varies on the land surface and at different soil depths (Moazenzadeh and Mohammadi 2019), but stations for recording T_s are often sparse and limited.

In recent years, indirect methods, including analytical, numerical, and data-driven models, have been suggested for accurate prediction of T_s. However, analytical models cannot reproduce the complex relationships between T_s and climatological variables, especially for different climates and global scales (Kang et al. 2000; Plauborg 2002). Numerical models use finite volume and finite element methods to solve heat transfer laws, and are highly complex (Badache et al. 2016; Samadianfard et al. 2018b). As an alternative, intelligence machine learning models can be used for predicting T_s and describing the interactions between T_s and other predictor variables, such as meteorological parameters (Moazenzadeh and Mohammadi 2019; Feng et al. 2019). Current advances in intelligence machine learning models are improving their capability for modeling non-linear relationships (Padarian et al. 2020).

Some machine learning approaches have been widely used in geosciences engineering and T_s prediction. These include artificial neural network (ANN) (Tabari et al. 2015; Sanikhani et al. 2018; Mehdizadeh et al. 2017; Kisi et al. 2017; Samadianfard et al. 2018a; Kazemi et al. 2018), multilayer perceptron (MLP) (Kim and Singh 2014; Kisi et al. 2015; Heddam, 2019; Sihag et al. 2020), radial basis function (RBF) (Kisi et al. 2015); general regression neural network (GRNN)

(Feng et al. 2019); extreme learning machine (ELM) (Nahvi et al. 2016; Sanikhani et al. 2018; Feng et al. 2019), support vector machine (SVM) (Xing et al. 2018; Delbari et al. 2019), wavelet neural network (WNN) (Araghi et al. 2017; Samadianfard et al. 2018a), adaptive neuron fuzzy inference system (ANFIS) (Talaee 2014; Abyaneh et al. 2016; Citakoglu 2017; Singh et al. 2018), M5 model tree (Sanikhani et al. 2018; Feng et al. 2019), and gene expression programming (GEP) (Mehdizadeh et al. 2017; Kisi et al. 2017; Samadianfard et al. 2018a). These models have proven useful in dealing with difficult non-linear and hidden relationships among input data, but often suffer from some weaknesses, such as easily falling into local optimums, membership function learning problems, over-fitting, and low convergence speed (Zhao et al. 2019; Mehdizadeh et al. 2020; Qasem et al. 2019).

To overcome the existing drawbacks of standalone machine learning approaches and obtain higher prediction accuracy, hybrid models can be used (Riahi-Madvar et al. 2020; Seifi and Soroush 2020). Hybrid methods apply nature-inspired meta-heuristic algorithms to optimize the performance of standalone models. Quick data-processing speed, achieving a global optimum, higher precision than standalone models, and robust generalization are some advantages of integrated machine learning-optimization algorithm techniques (Baydaroğlu and Koçak 2014; Moazenzadeh and Mohammadi 2019). For example, Nahvi et al. (2016) found that self-adaptive evolutionary (SaE) enhanced the estimation accuracy of ELM in predicting daily T_s at different soil depths based on air temperature (T_a), compared with the standalone ELM, GP, and ANN models. Samadianfard et al. (2018b) developed a coupled MLP-firefly algorithm (MLP-FFA) model for monthly T_s estimation in the 0-100 cm soil layer in Adana, Turkey, using the climate variables T_a, atmospheric pressure (P_a), and solar radiation (R_s), and found that it performed better than the standalone MLP model, especially at 20 cm soil depth. Moazenzadeh and Mohammadi

(2019) estimated daily T_s at six soil depths in Maragheh, Iran, using two standalone models, elman neural network (ENN) and support vector regression (SVR), and four coupled models, (SVR-FFA), SVR-krill herd algorithm (SVR-KHA), ENN-FFA, and ENN-KHA. They found that all models had their highest accuracy at 10 cm soil depth and that SVR-KHA showed the best estimation accuracy based on T_a, relative humidity (RH), and sunshine hours. Mehdizadeh et al. (2020b) hybridized the ENN model with two algorithms, ant colony optimization (ACO) and gravitational search algorithm (GSA), to predict daily T_s at four soil depths in Rasht and Isfahan, Iran, and found that ENN-GSA produced the most accurate predictions at all depths.

Hourly evaluation of T_s is essential for high-resolution modeling within hydrology, geosciences, ecology, and crop models as a decision-support system to achieve better crop yield (Qi et al. 2016; Sanikhani et al. 2018). Since hourly T_s measurement with instruments is difficult, previous studies have generally used daily or monthly datasets in T_s prediction. To our knowledge, few studies have investigated the precision of conventional machine learning models in predicting T_s at hourly scale (Araghi et al. 2017; Heddam 2019; Feng et al. 2019), while none has investigated model hybridization with integrated optimization algorithms to improve hourly T_s estimation in different climates.

Uncertainty analysis is a robust step to assess the reliability of different models (Seifi et al. 2020). Previous studies on T_s prediction are mostly based on standalone machine learning models and consider straightforward prediction, with no explicit investigation of the associated uncertainty and coherence analysis.

In this study, four machine learning models (ANFIS, MLP, SVM, and radial basis function neural network (RBFNN)) were used to predict hourly T_s at three soil depths in two climate zones. The models were then hybridized with four bio-inspired meta-heuristic algorithms (sunflower

optimization (SFO), salp swarm algorithm (SSA), FFA, particle swarm optimization (PSO)) and model parameter values optimizing the precision of the models were analyzed. In a further novel approach, generalized likelihood uncertainty estimation (GLUE) was applied in uncertainty analysis to compare the validity and reliability of the models.

Since inferring the relationships between climate variables (T_a, RH, wind speed (U), R_s) and hourly T_s data can lead to a better understanding of soil temperature response to model structure, wavelet coherence analysis was used to assess the behavior of hourly T_s at different soil depths relative to meteorological variables and to identify the most significant meteorological variable for these predictions. To our knowledge based on a literature review, no previous study has applied wavelet coherence analysis to T_s and other climate variables.

Despite the popularity of hybrid optimization models for daily and monthly T_s prediction, few studies have compared hybrid model precision in predicting hourly T_s, especially by analyzing related uncertainty and investigating significant meteorological factors. There have also been few accuracy evaluations of hybrid ANFIS and SVM models in estimating hourly T_s in Iran. The primary aims of this study were therefore to: 1) develop and compare ANFIS, MLP, RBFNN, and SVM hybridized with the SFO, SSA, FFA, and PSO algorithms in predicting hourly T_s at three soil depths in two climate zones; 2) select best values of optimization algorithm parameters, using the Taguchi method; 3) identify model uncertainty at different soil depths using the GLUE approach; and 4) determine the relationships between hourly T_s and T_a, U, RH, and R_s at different soil depths, using wavelet coherence analysis.

2- Material and Methods

2-1- Study area and dataset

Two datasets of measured hourly T_s were chosen to evaluate the hybrid and standalone models. The first dataset was obtained from an automatic monitoring station in a pistachio orchard (55˚82' N, 29˚30' E) in Sirjan city, Iran (Fig. 1), where information about T_s at soil depth is essential in disease control, evaporation modeling, irrigation management, and frost protection. Sirjan has an arid climate, with mean annual air temperature of 27˚C and mean annual rainfall of 40 mm. Hourly T_s and meteorological parameters (T_a, R_s, U, RH) in the field were monitored from 12 September 2012 to 17 January 2012. From a total of 1966 data obtained, 1500 hourly data were randomly selected for model learning and the remaining 466 hourly data were used for model testing.

The second T_s dataset was obtained from a synoptic station in Sanandaj (35.33°N, 47.00°E, 1373.4 m height), western Iran (Fig. 1). This region has a semi-humid climate, based on the calculated aridity index using 30-year meteorological data (Zolfaghari et al. 2016), with hot conditions in summer and very cold winters. Mean annual air temperature measured at Sanandaj station is 13.4˚C and mean annual rainfall is 450 mm. Hourly T_s and meteorological parameters (T_a, R_s, U, RH) were recorded from 9 July 2009 to 12 October 2009. A set of 800 hourly T_s data was randomly selected and used for learning the models, while 200 hourly T_s data were used for testing.

Time series plots of T_a and hourly T_s at three depths (5, 10, and 30 cm) in the soil at Sirjan and Sanandaj revealed that temperature variations showed a decreasing trend at all soil depths (Fig. 2). The greatest difference in temperature between initial and final points was at 5 cm soil depth (15˚C) in Sirjan, while in Sanandaj station, it was 21 ˚C at 10 cm and 19˚C at 30 cm soil depth. Statistical characteristics on the measured meteorological and T_s data are given in Table 1.

2-2- Adaptive neuron fuzzy inference system (ANFIS)

ANFIS is a type of ANN model combined with Takagi-Sugeno fuzzy, i.e., it uses both fuzzy logic and neural networks and can capture the advantages of both (Najafi-Ghiri et al. 2019). Two rules in the "if-then" method for the Takagi-Sugeno model were considered here (Njafi-Ghir et al. 2019):

$$Rule1: if\ x\ is\ A_1 and\ y\ is\ B_1, then\ f_1 = p_1x + q_1y + r_1 \quad (1)$$

$$Rule2: if\ x\ is\ A_2 and\ y\ is\ B_2, then\ f_2 = p_2x + q_2y + r_2 \quad (2)$$

where A_1, A_2, B_1, and B_2 are membership functions and p_1, q_1, r_1, and p_2, q_2, r_2 are consequence parameters.

The ANFIS structure contains five layers, where layers 1 and 4 include adaptive parameters and layers 2, 3, and 5 consist of non-adaptive nodes. In layer 1, each node adjusts to a function parameter and produces a value of membership degree ($\mu_{Ai}(x)\ and\ \mu_{B_{i-2}}(x)$). In layer 2, each node is defined and shows a firing strength for each rule (w_i). The outcome of multiplying the signals coming into the node is the output of each node. Normalized firing strength (NFS, $\bar{w}_i$) is created in the third layer as the ratio between the ith rule's firing strength (FS) and the total sum of FS for all rules. In the adaptive nodes of layer 4, the node function is defined as $O_{4,i} = \bar{w}_i f_i$. In layer 5, the overall output is calculated through combining all incoming signals as $y = \sum \bar{w}_i f_i$.

In this study, the bell membership function was used, due to its smoothness and brevity:

$$\mu_{Ai} = \frac{1}{1 + \left[\left(\frac{x - c_i}{a_i}\right)^2\right]^{b_i}}, i = 1,2 \quad (3)$$

where a_i, c_i, and b_i are premise parameters of membership functions.

2-3- Multilayer perceptron (MLP) model

MLP is a feedforward supervised neural network that has been applied successfully to complex problems. The backpropagation learning algorithm is commonly used for training MLP models, but it may get trapped in a local optimum (Pouladi et al. 2019). The MLP model uses multiple layers with a non-linear activation function to learn the relationship between input and output datasets. The first layer (input layer) contains the inputs to the MLP model, while the middle layers (hidden layers) contain a number of neurons. Each neuron performs a weighted summation of inputs. The activation functions are used to calculate the inner product of input parameters and adjustable weight vectors of synapses (Pouladi et al. 2019). More details about MLP can be found in Kisi et al. (2015).

2-4- Radial basis function neural network (RBFNN)

The RBFNN model is a particular type of ANN model that has been widely used for modeling hydrological variables such as streamflow, runoff, temperature, drought, and groundwater level. The main difference between RBFNN and feedforward multilayer ANN is the transfer function properties employed in the hidden layers (Walczak and Massart 2000). RBFNN contains three layers in its structure. The first layer receives the input vector data, where the hidden layers include several nodes and a nonlinear transfer function (Tayebi et al. 2019). The Euclidean norm (distance) associated with the hidden layer's input vector and center is computed by the activation function related to each hidden neuron. Commonly, the hidden layers contain the nonlinear radial basis Gaussian function and another activation function placed in the last layer. More details about RBFNN can be found in Kisi et al. (2015).

2-5- Support vector machine (SVM)

SVM was initially introduced by Cortes and Vapnik (1995) and has been widely used for both regression and classification analysis, due to its advantage in minimizing model complexity and estimation error simultaneously (Vapnik 1999; Zheng et al. 2020). The SVM model uses different kernel functions to estimate the regressions, implicitly converting inputs to high-dimensional feature space using a hyper-plane (Xing et al. 2018). The SVM equation is:

$$f(X_i) = \omega^T . \varphi(X_i) + b \tag{4}$$

where $f(X_i)$ is a deterministic function, $\varphi(x_i)$ is a non-linear transferring the input vector, ω is a vector of weight coefficients, and b is bias.

The b and ω values are determined by minimizing risk structure-function. To reduce the complexity and obtain a more robust model, slack variables ξ_i, ξ_{i^*} can be used in the risk structure-function equation:

$$Minimize \left(\frac{1}{2}\right) \|\omega\|^2 + C_0 \sum_{i=1}^{M} (\xi_i + \xi_{i^*}) \tag{5}$$

$$subject\ to = \begin{bmatrix} y_i - (\langle \omega, \psi(X_i) \rangle + b) \leq \varepsilon + \xi_i \\ (\langle \omega, \psi(X_i) \rangle + b) - y_i < \varepsilon + \xi_{i^*} \end{bmatrix}$$

where ε is intensive loss value, $y_i$is the ith output, and $C_0$is the cost constant.

Lagrange multipliers (α_i and α_{i^*}) can be applied for solving eq. 5, with the solution written as follows using kernel function ($K(X_i, X)$):

$$f(X_i) = \sum_{i=1}^{M} (\alpha_i - \alpha_{i^*}) K(X_i, X) + b \tag{6}$$

The radial basis function ($K(X_i, X) = exp(-\gamma \|X_i - X\|^2)$) is widely used for SVM models.

2-6- Sunflower optimization algorithm (SFO)

SFO is a new optimization algorithm proposed by Yang (2012) inspired by the solar tracking of sunflower heads to enhance pollination. SFO uses inverse square law radiation (ISLR) for optimization, based on the simple assumption that each flower only generates one gamete of pollen and reproduces individually (Qias et al. 2019). When the sunlight falls more obliquely, the sunflower receives less heat from the sun, expressed by the ISLR as:

$$Q_i = \frac{P}{4\pi r_i^2} \tag{7}$$

where P is the power of source and r_i is the distance between the current and the best i plant.

The redirection of position by the sunflower is computed as:

$$d_i = \lambda \times P_i(\|X_i + X_{i-1}\|) \times \|X_i + X_{i-1}\| \tag{8}$$

where λ is the inertial displacement of the sunflower and is constant, $X^*$is the best location of the sunflower, and X_i is the current location of the plant, and $P_i(\|X_i + X_{i-1}\|)$ is the pollution probability, where i^{th} sunflower cross-pollinates with another near $i\text{-}1^{th}$ sunflower to generate a new individual in an updated location.

It is essential to limit the maximum step of individuals by:

$$d_{\max} = \frac{\|X_{\max} - X_{\min}\|}{2 \times N_{pop}} \tag{9}$$

where d_{max} is the maximum step, X_{max} is the upper bound value, X_{min} is the lower bound value, and N_{pop} is the number of sunflowers in the overall population.

Finally, the next population is updated as:

$$\vec{X}_{i+1} = \vec{X}_i + d_i \times \vec{s}_i \tag{10}$$

$$\vec{s}_i = \frac{X^* - X_i}{\|X^* - X_i\|} \tag{11}$$

where $\vec{X}_{i+1}$is the position of sunflower $i+1$.

2-7- Firefly algorithm (FFA)

FFA was first developed by Yang (2010), inspired by the light emission capability of fireflies. The attractiveness of one firefly to another is related to its brightness to neighboring fireflies, where a less bright firefly is attracted to a brighter one (Alor et al. 2019; Riahi-Madvar et al. 2020). The excellent information-sharing mechanism is one of the advantages of FFA. The firefly mechanism is formulated as:

$$I(r_{ij}) = I_0 e^{-\gamma r_{ij}^2} \tag{12}$$

$$\beta(r_{ij}) = \beta_0 e^{-\gamma r_{ij}^2} \tag{13}$$

where $\beta(r_{ij})$ is the attractiveness of a firefly, β_0 is the attractiveness of firefly at $r=0$, γ is the absorption coefficient in the range of 0 and 1, $I(r_{ij})$ is the light intensity, I_0 is the light intensity at $r=0$, and the distance between two fireflies i, j at locations of x_i and x_j can be defined as $r_{ij} = \|x_i - x_j\|$. The firefly i is attracted by firefly j and updates its location as:

$$\Delta x_i = \beta_0 e^{-\gamma r^2}\left(x_j^t - x_i^t\right) + \varsigma\mu \tag{14}$$

$$x_i^{t+1} = x_i^t + \Delta x_i$$

where ς is randomization parameter, and μ is a vector of random parameters.

2-8- Salp swarm algorithm (SSA)

SSA is a new meta-heuristic optimization algorithm, inspired by the collective behavior of salps (sea squirts), introduced by Mirjalili et al. (2017). Adaptability, robustness, and scalability are the most important advantages of SSA. Based on the individual's location in the chain, salps are divided into leaders or followers in SSA. The followers follow the leader to guide them in their movements. The SSA starts by initializing the salp population. The leader position is updated as:

$$x_i^l = \begin{bmatrix} y_i + r_1\left((ub_i - lb_i)r_2 + lb_i\right) \leftarrow r_3 \geq 0 \\ y_i + r_1\left((ub_i - lb_i)r_2 + lb_i\right) \leftarrow r_3 < 0 \end{bmatrix} \quad (15)$$

where x_i^l is the leader's position, y_i is the food source, lb_i and ub_i are the lower and upper bounds, respectively, r_3 and r_2 are random numbers, and r_1 is computed as:

$$r_1 = 2e^{-\left(\frac{4l}{L}\right)} \quad (16)$$

where l is the existing iteration, and L is the maximum number of iterations. SSA uses the parameter r_1 to increase stability in exploration and exploitation capability. For each follower, the position is updated as:

$$x_j^i = \frac{1}{2}\left(x_j^i + x_j^{i-1}\right) \quad (17)$$

where x_j^i is the location of jth salp in the ith dimension.

2-9- Particle swarm optimization (PSO)

PSO is a well-established stochastic/random search approach related to the swarm and inspired by the particle's social behavior. Each particle in the swarm protects the updating of search behavior in accordance with learning experiences of all other particles. In each generation, information is integrated by particles to set the velocity on every dimension. The position and velocity of particles are updated as:

$$v_{i,t+1} = \eta * v_{i,t} + c_1 * rand * \left(p_{i,t} - x_{i,t}\right) + c_2 * rand * \left(p_{g,t} - x_{i,t}\right) \quad (18)$$

$$x_{i,t+1} = x_{i,t} + v_{i,t+1} \quad (19)$$

where $v_{i,t+1}$ is the velocity of i^{th} particle at iteration $t+1$, η is the weight inertia, c_1 and c_2 are acceleration coefficients, $x_{i,t+1}$ is the location of i^{th} particle at iteration $t+1$, $p_{i,t}$ is the optimal location experienced by particles, and $p_{g,t}$ is the optimal location experienced by any particle.

2-10- Hybridizing ANFIS, MLP, RBFNN, and SVM with optimization algorithms

In this study, SFO, FFA, SSA, and PSO were used to fine-tune the parameters of the ANFIS, MLP, RBFNN, and SVM models. The input data were entered for training. The optimization algorithms then started with random selection of agents (particles, fireflies, salps, and sunflowers) and finally determined each individual's position. The position of agents shows: the values of the premise (a_i, b_i, c_i) and consequent (p_1, q_1, r_1, p_2, q_2, r_2) parameters in the ANFIS model; the values of bias and weight connections for the MLP model; the width values and the hidden neuron center in the RBFNN model; and the values of width (γ), penalty (C), epsilon (ε), and kernel function parameters in the SVM model. The algorithms used their operators to update the position of each agent. The initial values of the parameters were regarded as the initial positions of agents. The objective function of root mean square error (RMSE) was applied to verify model accuracy. The hybrid ANFIS, MLP, RBFNN, and SVM models continued until the minimum value of RMSE was detected. The optimal values of the premise and consequent parameters were found in each update of the agents' position.

Robust design of random parameters included in the optimization algorithms is important to enhance model performance. In a novel approach, Taguchi search was used in this study for selecting the best values of these random parameters. It is a powerful advanced technique that uses orthogonal array and signal to noise ratio (S/N) to minimize the number of experiments and greatly decrease the time, cost, and effort in finding optimal parameters of algorithms (Zhang et al. 2015). An orthogonal array table is created by calculating total degree of freedom (DOF) based on the combined degree of freedom of all parameters (Canbolat et al. 2019; Bademlioglu et al. 2020). Based on number of levels (L) and number of parameters (NV), the total number of experiments needed to find the optimum level of parameters is computed. The minimum number of experiments (N) is calculated as $N = 1 + NV(L - 1)$. Thus e.g., for the four parameters with four levels in the

PSO algorithm, at least 13 experiments should be conducted to discover the optimal values of PSO parameters, while without the Taguchi method, the total number of experiments would be 4^4. Thus, the Taguchi orthogonal array of L16 (4^3) was established.

The S/N ratio is calculated as:

$$\frac{S}{N} = -10log\left(\frac{1}{n}\sum_{i=1}^{n}\frac{1}{y_i^2}\right) \tag{20}$$

where *n* is the number of the case, and *y* is the performance characteristic performance value (the higher the S/N value, the better the ratio). S/N was used as a performance characteristic of each parameter in this study.

The framework and flowchart of the work in this study is presented in Fig. 3, which also shows the general framework of the 16 hybrid models used to predict hourly T_s (ANFIS-SFO, ANFIS-FFA, ANFIS-SSA, ANFIS-PSO, MLP-SFO, MLP-FFA, MLP-SSA, MLP-PSO, RBFNN-SFO, RBFNN-FFA, RBFNN-SSA, RBFNN-PSO, SVM-SFO, SVM-FFA, SVM-SSA, and SVM-PSO).

2-11- Evaluation criteria

Coefficient of determination (R^2), RMSE, Nash-Sutcliffe efficiency (NSE), mean absolute error (MAE), and percentage bias (PBIAS) were used to assess the accuracy of the standalone and hybrid models (Moriasi et al. 2007; Moriasi et al. 2015):

$$R^2 = \frac{\sum_{i=1}^{n}(x_i - \bar{x})(y_i - \bar{y})}{\sqrt{(\sum_{i=1}^{n}(x_i - \bar{x})^2(\sum_{i=1}^{n}(y_i - \bar{y})^2))}} \qquad optimal\ value: 1 \tag{21}$$

$$RMSE = \sqrt{\sum_{i=1}^{n}\frac{(x_t - y_t)^2}{N}} \qquad optimal\ value: 0 \tag{22}$$

$$MAE = \sum_{i=1}^{i=N} \frac{|x_i - y_i|}{N} \qquad optimal\ value: 0 \tag{23}$$

$$NSE = 1 - \frac{\sum_{i=1}^{N}(x_t - y_t)^2}{\sum_{i=1}^{N}(x_t - \bar{x}_t)} \qquad optimal\ value: 1 \tag{24}$$

$$PBIAS = \left[\frac{\sum_{i=1}^{N}(x_i - y_i) * 100}{\sum_{i=1}^{N}(x_i)}\right] \qquad optimal\ value: 0 \tag{25}$$

GLUE analysis was performed to investigate model reliability. The analysis has three important levels (Viola et al. 2009; Sun et al. 2016):

Level 1: Random sampling is used to create a large number of sampling sets from a prior distribution of input data.

Level 2: Likelihood value is calculated from model runs and compared with a certain threshold value to evaluate each input parameter as behavioral (value above the threshold likelihood) or non-behavioral (value below the threshold likelihood). Behavioral parameters are retained to judge the models. Likelihood is calculated as:

$$L(\theta_i|Y) = exp\left[\frac{-N\sigma_i^2}{\sigma_{obs}^2}\right] \tag{26}$$

where N is adjustable parameter, σ_i^2 is the error variance for the i^{th} model, σ_{obs} is the variance of observations, θ_i is the parameter set, and $L(\theta_i|Y)$ is the likelihood measure for the i^{th} model calculated with the observations Y.

Level 3: Simulation weights for behavioral parameter sets are rescaled and the cumulative weighted distribution of estimations is used in quantile estimation for uncertainty prediction:

$$\vartheta_i = \frac{L(\theta_i)}{\sum_{k=1}^{n} L(\theta_k)} \tag{27}$$

where ϑ_i is a likelihood weight and n is the number of data.

Two indices, p and r, are used to quantify model uncertainty, where p is percentage of bracketed observations at 95% prediction uncertainty (95PPU) and r is mean 95PPU range, separated using the standard deviation of observations (Seifi et al. 2020):

$$\bar{d}_x = \frac{1}{k}\sum_{l=1}^{k}(X_U - X_L) \quad , \quad r = \frac{\bar{d}}{\rho_x} \tag{28}$$

where k is the number of observations, ρ_x is the standard deviation of observations, and X_U and X_L are the upper and lower boundary of the 95% prediction uncertainty, respectively. Lower values of r and higher values for p indicate lower uncertainty. In this study, the spectral responses of models in the GLUE technique were used to assess variations in r and p.

2-12- Wavelet coherence analysis in interaction analysis

In reality, T_s is tele-connected to different meteorological variables such as T_a, RH, U, and R_s. Wavelet coherence analysis was used here to assess these interactions. It calculates the coherence value of cross-wavelet transform among two time series in the time-frequency domain (Lee and Kim 2019). Detailed theory on wavelet transform can be found in Grinstead et al. (2004). In the present case, wavelet coherence between T_s and meteorological variables was calculated as (Lee and Kim 2019):

$$Coherence = \frac{\left|S\left(s^{-1}W_i^{xy}(s)\right)\right|^2}{S(s^{-1}|W_i^x(s)|^2)S\left(s^{-1}|W_i^y(s)|^2\right)} \tag{29}$$

$$|W_i^{xy}| = \left|W_i^x \bar{W}_i^Y(s)\right| \tag{30}$$

$$S(W) = S_{scale}\left(S_{time}\left(W(s,\tau)\right)\right) \tag{31}$$

where x and y are two time series, s is the smoothing over both scale and time, S is smoothing operator, W_i^x is the wavelet coefficient of soil temperature and meteorological parameters in the time series x, W_i^y is the wavelet coefficient of soil temperature and meteorological parameters in

the time series y, $W_i^{xy}(s)$ is the cross-wavelet power spectrum of x and y, τ is the occasion, S_{scale} is smoothing along with the wavelet, and $S_{time}$is smoothing in time (see Fig. 4).

3- Results and discussion

The best optimization algorithm parameters, extracted with Taguchi search, for training the standalone and hybrid models to predict T_s based on climate variables (T_a, R_s, U, RH) are presented in section 3.1. In section 3.2, model performance and the results obtained at different sites and soil depths are compared. The uncertainty associated with the simulations, determined using the GLUE approach, is presented in section 3.3. Wavelet coherence results for the interconnections between T_s and climate variables are summarized in section 3.4.

3-1- Optimal model parameters derivation by Taguchi search

The optimization parameters of the meta-heuristic algorithms combined with SFO, SSA, FFA, and PSO at different levels, and the associated S/N values, are shown in Table 2. The values of population size, c_1, c_2, inertia weight, and γ in optimization algorithms were derived based on the Taguchi method. After constructing an orthogonal array and calculating S/N ratio for each algorithm parameter, the optimal values were chosen (highest S/N ratio) (Table 2). The effect of each optimization algorithm process parameter was divided into four levels. For the PSO algorithm, the mean value of RMSE for population size varied from 1.12 to 1.54, inertia weight from 1.23 to 1.76, c_1 from 1.12 to 1.45, and c_2 from 1.37 to 1.45, and the best conditions were obtained at a value of 2, 4, 1, and 1, respectively. The greatest variation in S/N values was seen for inertia weight, i.e. PSO was mainly affected by inertia weight, which should be the main focus in model development. The most critical parameter for SSA, SFO, and FFA was r_3, population size,

and γ, respectively. The optimal value of r_3, r_2, and population size for SSA, determined by Taguchi search, was 0.5, 0.8, and 400 respectively. For SFO, population size of 400 was most effective, while for FFA γ had an optimal value of 0.8. These results indicate that Taguchi search can effectively and systematically provide robustness values in selection of optimization parameters, replacing the trial-and-error approach. It can be used in future studies of meta-heuristics to improve the ability and applicability of models.

3-2- Performance analysis of models

The performance of standalone ANFIS, MLP, RBFNN, and SVM and the hybrid models was evaluated based on statistical criteria and by comparison of predictions against measured hourly T_s at 5, 10, and 30 cm soil depth (Tables 3 and 4). Soil temperature was used as the target parameter, and corresponding T_a, U, R_s, and RH as input data for all models. At the training level, integration of SFO with ANFIS, SVM, RBFNN, and MLP led to better results. The standalone ANFIS model outperformed the other standalone SVM, RBFNN, and MLP models. All models provided the highest accuracy at 10 cm soil depth, and the lowest at 5 cm soil depth. The prediction accuracy in terms of RMSE, MAE, NSE, and PBIAS for the training level was lower for SVM-PSO than for the other hybrid ANFIS, SVM, MLP, and RBFNN models.

It should be noted that the measured data at 5 cm depth were from the arid Sirjan site and the measured data at 10 and 30 cm soil depths from the semi-humid Sanandaj site. Table 4 shows the performance of the models in predicting hourly T_s in terms of RMSE (°C), MAE (°C), PBIAS (%) (optimal value=0), and NSE (optimal value=1) in the testing phase. Scatter plots and correlation comparisons between simulated and measured T_s' values at 5, 10, and 30 cm soil depths are presented in Fig. 5, 6, and 7, respectively. At 5 cm depth, ANFIS-SFO had the lowest error of all

hybrid models (RMSE=1.18, MAE=1.05, PBIAS=7). ANFIS-SFO also had the lowest error of all models at 10 cm depth (RMSE=0.824, MAE=0.822, PBIAS=1, NSE=0.98) and at 30 cm depth (RMSE=0.911, MAE=0.905, PBIAS=2, NSE=0.97) (Table 4).

The ANFIS model was the most accurate of the standalone models, with RMSE=0.978 ^{o}C, MAE= 0.971 ^{o}C, NSE=0.85, and PBIAS=14% in the best case (at 10 cm soil depth). The ANFIS model has been shown previously to be superior in T_s prediction. For example, Citacogle (2016) reported that ANFIS was better (MAE=1.09, RMSE=1.99, R^2=0.98) than the ANN model in estimating hourly T_s when using monthly minimum temperature, monthly maximum temperature, calendar month number, soil depth, and monthly precipitation as input data. As can be seen from Table 4, the SVM model had the highest error (highest MAE, RMSE, and PBIAS values, lowest NSE values) of all models at all soil depths. Nanda et al. (2020) also found that SVM had the lowest precision of all machine learning models tested in hourly and half-hourly T_s prediction. The main reason for the low accuracy of SVM may be non-linearity between several analyzed parameters.

Comparison of the results at 10 and 30 cm depth indicated that the error in T_s estimation increased with depth, indicating that meteorological parameters mostly influenced soil temperature in the upper layers (Kazemi et al. 2018; Behmanesh and Mehdizadeh, 2017). Similarly, Nahvi et al. (2016) found that the precision of machine learning models in estimation of T_s in soils in Turkey and Iran declined from 10 cm to 100 cm depth, but increased from 5 to 10 cm depth. Behmanesh and Mehdizadeh (2017) also found that the accuracy of machine learning models increased between 5 and 10 cm depth. In the present study, the highest accuracy was observed at 10 cm depth for all hybrid and standalone models, as also found by e.g., Behmanesh and Mehdizadeh (2017) and Kisi et al. (2017). Among the models they studied, Kisi et al. (2017) found that ANFIS

achieved the highest precision at 10 cm depth (RMSE=1.29) based on 25-year monthly dataset at 10, 50, and 100 cm depth.

Based on the results in Table 4, in this study the SFO algorithm increased the accuracy of standalone models most, decreasing RMSE by 5.6% for ANFIS-SFO and 18.3% for RBFNN-SFO, both at 5 cm depth. The SSA algorithm decreased RMSE by 6.2% at 10 cm depth for MLP-SSA and 15% for RBFNN-SSA at 5 cm depth. The FFA algorithm decreased RMSE by 3.3% at 10 cm depth for MLP-FFA and 10.9% at 5 cm depth for SVM-FFA. Similarly, Samadianfard et al. (2018) found that integrated MLP-FFA and SVM-FFA models had significantly higher T_s prediction accuracy compared with the standalone MLP and SVM models at 5, 10, and 20 cm soil depth.

In the scatterplots of all test dataset, all estimations fell on the 1:1 line, with R^2 values >0.99 for all models (Figs. 5-7). The R^2 value increased from 0.9958 to 0.9998, 0.9934 to 0.9993, and 0.9950 to 0.9998 for all hybrid and standalone models at 5, 10, and 30 cm depth, respectively. All models had the most accurate performance for 10 cm soil depth and the worst for 5 cm soil depth (Figs. 5-7). This reflects the complexity and rapid changes in T_s at shallow depths. Overall, the ANFIS-SFO predictions were closest to the observed data, with the highest R^2 and lowest error at each soil depth, confirming the suitability of ANFIS-SFO for estimating hourly T_s in regions with arid (Sirjan) and semi-humid (Sanandaj) climates.

From Table 4 and Figures 5-7, it is evident that use of the all meta-heuristic algorithms (SFO, SSA, FFA, PSO) improved the accuracy of the corresponding standalone models. This may be due to more accurate searching and finding the best solution in the local and global spaces. This is in agreement with findings by Mehdizade et al. (2020), Moazenzadeh and Mohammadi (2019) and Shamshirband et al. (2020) that hybrid models show higher accuracy than conventional models. Based on results from the present study, the ANFIS model integrated with a meta-heuristic

optimization algorithm is highly recommended for estimating T_s at different soil depths in different climates.

3-3- Uncertainty analysis of models

Spectral representations of uncertainty values of the models at the testing level for 5, 10, and 30 cm soil depth, determined using the GLUE approach, are shown in Fig. 8. At 5 cm soil depth, the *r* value for the testing data for ANFIS-SFO ranged from 0.10 to 0.15 with 486-972 data points and from 0.15 to 0.20 with 1458-1944 data points. The *p* value at 5 cm soil depth for ANFIS-SFO was found to be 0.95 with 486-972 data points. For 10 and 30 cm soil depth, the *p* range for ANFIS-SFO was 0.90-0.94 and 0.92-0.96, respectively. The uncertainty analysis showed *p* values in the range 0.86-0.90 and 0.86-0.90 for MLP-SFO and RBFNN-SFO, respectively, with 600-1000 data points. ANFIS-PSO, MLP-PSO, RBFNN-PSO, and SVM-PSO had higher *r* and lowest *p* than other hybrid models. ANFIS-SFO and MLP-SFO had the highest bracketed observed values in the testing level, while the lowest unbracketed observations were obtained with the standalone SVM and RBFNN models. This indicates that using meta-heuristic algorithms such as SFO results in certain parameter adjustment in AI models and reduces the case-specificity, improving the generality of the models. In the present case, hybridization of the model decreased the uncertainty in soil temperature predictions and provided more accurate and reliable depth analysis of temperature.

In the uncertainty analysis, an increase in the number of data points increased the *r* values for the different models (Fig. 8). In general, SVM had the highest *r* and lowest *p*, indicating a high level of uncertainty. The standalone and hybrid MLP models produced more accurate predictions than the standalone and hybrid RBFNN models. Overall, the optimization algorithms improved the

performance and reliability of the standalone models in terms of *r* and *p* values. SFO outperformed the other optimization algorithms in reducing uncertainty in estimation of hourly T_s at all soil depths.

In general, the evaluation criteria values and GLUE uncertainty analysis of models confirmed that the hybrid ANFIS-SFO model had most accurate performance in predicting hourly T_s based on T_a, RH, U, and R_s for semi-humid and arid climates of Iran. The results demonstrated the suitability of SFO for hybridizing machine learning models.

3-4- Wavelet coherence analysis

To assess the importance of input vector selection in T_s simulation, the effect of four meteorological parameters was considered using wavelet coherence analysis. The wavelet coherence between T_s and other climate variables (T_a, U, R_s, and RH) at 5, 10, and 30 soil depths is shown in Figures 9 and 10 for the period 0-1944 hours at 5 cm soil depth and 0-1000 hours at 10 and 30 cm soil depth. There was high coherence between T_a and T_s at periodicity of 4-8 hours in the time domain 486-709 hours at 5 cm soil depth at Sirjan (Fig. 9). Overall, T_a showed the highest correlation with T_s, confirming findings by Kisi et al. (2015) and Nanda et al. (2020). Analysis of the diagram indicated no significant coherence between U and T_s at different time periodicities, but there was a significant relationship between T_s and R_s at periodicity of 28-34 hours, and between T_s and RH at periodicity of 28-34 hours, in the time domain 1252-1944 hours (Fig. 9). Overall, T_a, R_s, and RH showed variable coherence signals, while no significant coherence signal was observed at different periodicities for U. Using WNN models, Samadianfard et al. (2018a) demonstrated that T_a and R_s have unquestionable effects on T_s prediction at 5, 10, 20, 30, 50, and 100 soil depth at a synoptic station in Iran.

To further analyze the results of wavelet coherence, the values were plotted against periodicity of T_s. Fig. 10 shows the coherence at 10 and 30 cm soil depth for Sanandaj station. The maximum coherence between T_s at 10 and 30 cm soil depth and T_a was 0.8 and 0.7, respectively, at periodicity 8-16 hours in the time domain 0-1000 hours. There were no significant coherences between T_s at different periodicities and U at 10 and 30 cm soil depth. The maximum coherence between T_s at periodicity 4-8 hours and R_s in the time domain 0-1000 hours was 0.9 and 0.7 at 10 and 30 cm depth, respectively. The highest coherence found (0.9) was at 10 cm soil depth between RH and T_s at periodicity 8-16 hours in the time domain 0-1000 hours. These results indicate that wavelet coherence analysis can provide more quantitative evidence on periodicity and interaction of T_s with climate parameters at different soil depths.

4- Conclusions

Soil temperature strongly affects soil biological processes, irrigation scheduling, plant growth, the environment, and water resource management, but measuring soil temperature is time-consuming and costly. Accurate, reliable and certain prediction of soil temperature using models is thus necessary in agricultural, environmental and geosciences practices.

In this study, the machine learning models ANFIS, MLP, RBFNN, and SVM were used for estimating hourly soil temperature at various soil depths, based on meteorological data from an arid site (Sirjan) and a semi-humid site (Sanandaj) in Iran. Four meta-heuristic optimization algorithms (SFO, FFA, PSO, SSA) were used to hybridize and optimize the standalone models. Parameter selection of the meta-heuristic models was optimized by Taguchi search, while uncertainty in model results was analyzed by the GLUE approach. Wavelet coherence analysis was used to infer the interactional periodicity of variables.

ANFIS was the most accurate standalone model, while SVM was the least accurate, for both sites and all soil depths (5, 10, 30 cm). The optimization algorithms SFO and SSA were best in enhancing performance for all standalone models. Uncertainty results indicated that the bracketed observed values of the best model, ANFIS-SFO, were in the range 94-96%.

Coherence wavelet analysis indicated weak effects of wind speed, but strong effects of air temperature, relative humidity, and solar radiation, on temperature in upper layers. Periodicity of T_s with other effective parameters was inferred.

The approach developed in this study proved reliable and accurate for hybrid meta-heuristic model development and assessment. It is applicable in regions with similar climate conditions to the study sites. Future studies should consider the effects of climate scenarios on soil temperature for the base period and future period. ANIFS, SVM, RBFNN, and MLP can also be hybridized with multi-objective optimization algorithms to determine the optimal values of hyperparameters and appropriate inputs to the models.

Ethics declarations

Ethical approval

Not applicable.

Competing interests

The authors declare that they have no conflict interest.

Research involving human participants and/or animals

Not applicable.

Consent to participate

All authors have given consent to their contribution.

Consent to publish

All authors have agreed with the content and all have given explicit consent to publish.

Data availability

The datasets used and/or analyzed during the current study are available from the corresponding author on reasonable request.

Code availability

The code is available from the corresponding author on reasonable request.

Funding

Not applicable.

Contributions

Conceptualization: Akram Seifi, Mohammad Ehteram; Methodology: Akram Seifi, Mohammad Ehteram, Formal analysis and investigation: Akram Seifi, Mohammad Ehteram, Fatemeh Soroush, Fatemeh Nayebloei , Writing original draft preparation: Akram Seifi, Fatemeh Soroush, Fatemeh Nayebloei, Bahram Gharabaghi, Ali Torabi Haghighi

References

Abyaneh, H. Z., Varkeshi, M. B., Golmohammadi, G., & Mohammadi, K. (2016). Soil temperature estimation using an artificial neural network and co-active neuro-fuzzy inference system in two different climates. *Arabian Journal of Geosciences*, *9*(5), 377.

Alizamir, M., Kim, S., Zounemat-Kermani, M., Heddam, S., Shahrabadi, A. H., & Gharabaghi, B. (2020). Modelling daily soil temperature by hydro-meteorological data at different depths using a novel data-intelligence model: deep echo state network model. *Artificial Intelligence Review*, 1-28. DOI: 10.1007/s10462-020-09915-5.

Alor, A., Mota, D., Olmos-Sánchez, K., & Rodas-Osollo, J. (2019). An Order-Picking Model Associated With Hospital Components and Solved by a Firefly Algorithm. In Handbook of Research on Metaheuristics for Order Picking Optimization in Warehouses to Smart Cities (pp. 173-188). IGI Global.

Araghi, A., Mousavi-Baygi, M., Adamowski, J., Martinez, C., & van der Ploeg, M. (2017). Forecasting soil temperature based on surface air temperature using a wavelet artificial neural network. *Meteorological Applications*, *24*(4), 603-611.

Badache, M., Eslami-Nejad, P., Ouzzane, M., Aidoun, Z., & Lamarche, L. (2016). A new modeling approach for improved ground temperature profile determination. *Renewable Energy*, *85*, 436-444.

Bademlioglu, A. H., Canbolat, A. S., & Kaynakli, O. (2020). Multi-objective optimization of parameters affecting Organic Rankine Cycle performance characteristics with Taguchi-Grey Relational Analysis. *Renewable and Sustainable Energy Reviews*, *117*, 109483.

Baydaroğlu, Ö., & Koçak, K. (2014). SVR-based prediction of evaporation combined with chaotic approach. *Journal of Hydrology*, *508*, 356-363.

Behmanesh, J., & Mehdizadeh, S. (2017). Estimation of soil temperature using gene expression programming and artificial neural networks in a semiarid region. *Environmental Earth Sciences*, *76*(2), 76.

Bonakdari, H., Moeeni, H., Ebtehaj, I., Zeynoddin, M., Mahoammadian, A., & Gharabaghi, B. (2019). New insights into soil temperature time series modeling: linear or nonlinear?. *Theoretical and Applied Climatology*, *135*(3-4), 1157-1177. DOI: 10.1007/s00704-018-2436-2.

Canbolat, A. S., Bademlioglu, A. H., Arslanoglu, N., & Kaynakli, O. (2019). Performance optimization of absorption refrigeration systems using Taguchi, ANOVA and Grey Relational Analysis methods. *Journal of Cleaner Production*, *229*, 874-885.

Citakoglu, H. (2017). Comparison of artificial intelligence techniques for prediction of soil temperatures in Turkey. *Theoretical and Applied Climatology*, *130*(1-2), 545-556.

Cortes, C., & Vapnik, V. (1995). Support-vector networks. *Machine learning*, *20*(3), 273-297.

Delbari, M., Sharifazari, S., & Mohammadi, E. (2019). Modeling daily soil temperature over diverse climate conditions in Iran—a comparison of multiple linear regression and support vector regression techniques. *Theoretical and Applied Climatology*, *135*(3-4), 991-1001.

Feng, Y., Cui, N., Hao, W., Gao, L., & Gong, D. (2019). Estimation of soil temperature from meteorological data using different machine learning models. *Geoderma*, *338*, 67-77.

Grinsted, A., Moore, J. C., & Jevrejeva, S. (2004). Application of the cross wavelet transform and wavelet coherence to geophysical time series.

Heddam, S. (2019). Development of air–soil temperature model using computational intelligence paradigms: artificial neural network versus multiple linear regression. *Modeling Earth Systems and Environment*, *5*(3), 747-751.

Kang, S., Kim, S., Oh, S., & Lee, D. (2000). Predicting spatial and temporal patterns of soil temperature based on topography, surface cover and air temperature. *Forest Ecology and Management*, *136*(1-3), 173-184.

Kazemi, S. M. R., Minaei Bidgoli, B., Shamshirband, S., Karimi, S. M., Ghorbani, M. A., Chau, K. W., & Kazem Pour, R. (2018). Novel genetic-based negative correlation learning for estimating soil temperature. *Engineering Applications of Computational Fluid Mechanics*, *12*(1), 506-516.

Kim, S., & Singh, V. P. (2014). Modeling daily soil temperature using data-driven models and spatial distribution. *Theoretical and applied climatology*, *118*(3), 465-479.

Kisi, O., Sanikhani, H., & Cobaner, M. (2017). Soil temperature modeling at different depths using neuro-fuzzy, neural network, and genetic programming techniques. *Theoretical and Applied Climatology*, *129*(3-4), 833-848.

Kisi, O., Tombul, M., & Kermani, M. Z. (2015). Modeling soil temperatures at different depths by using three different neural computing techniques. *Theoretical and applied climatology*, *121*(1-2), 377-387.

Lee, E., & Kim, S. (2019). Wavelet analysis of soil moisture measurements for hillslope hydrological processes. *Journal of Hydrology*, *575*, 82-93.

Lehnert, M. (2014). Factors affecting soil temperature as limits of spatial interpretation and simulation of soil temperature. *Acta Universitatis Palackianae Olomucensis–Geographica*, *45*(1), 5-21.

Mehdizadeh, S. (2018). Estimation of daily reference evapotranspiration (ETo) using artificial intelligence methods: Offering a new approach for lagged ETo data-based modeling. *Journal of hydrology*, *559*, 794-812.

Mehdizadeh, S., Behmanesh, J., & Khalili, K. (2017). Evaluating the performance of artificial intelligence methods for estimation of monthly mean soil temperature without using meteorological data. *Environmental Earth Sciences*, *76*(8), 325.

Mehdizadeh, S., Fathian, F., Safari, M. J. S., & Khosravi, A. (2020a). Developing novel hybrid models for estimation of daily soil temperature at various depths. *Soil and Tillage Research*, *197*, 104513.

Mehdizadeh, S., Mohammadi, B., Pham, Q. B., Khoi, D. N., & Linh, N. T. T. (2020b). Implementing novel hybrid models to improve indirect measurement of the daily soil temperature: Elman neural network coupled with gravitational search algorithm and ant colony optimization. *Measurement*, *165*, 108127.

Mirjalili, S., Gandomi, A. H., Mirjalili, S. Z., Saremi, S., Faris, H., & Mirjalili, S. M. (2017). Salp Swarm Algorithm: A bio-inspired optimizer for engineering design problems. *Advances in Engineering Software*, *114*, 163-191.

Moazenzadeh, R., & Mohammadi, B. (2019). Assessment of bio-inspired metaheuristic optimisation algorithms for estimating soil temperature. *Geoderma*, *353*, 152-171.

Moriasi, D. N., Arnold, J. G., Van Liew, M. W., Bingner, R. L., Harmel, R. D., & Veith, T. L. (2007). Model evaluation guidelines for systematic quantification of accuracy in watershed simulations. *Transactions of the ASABE*, *50*(3), 885-900.

Moriasi, D. N., Gitau, M. W., Pai, N., & Daggupati, P. (2015). Hydrologic and water quality models: Performance measures and evaluation criteria. *Transactions of the ASABE*, *58*(6), 1763-1785.

Nahvi, B., Habibi, J., Mohammadi, K., Shamshirband, S., & Al Razgan, O. S. (2016). Using self-adaptive evolutionary algorithm to improve the performance of an extreme learning machine for estimating soil temperature. *Computers and Electronics in Agriculture*, *124*, 150-160.

Najafi-Ghiri, M., Mokarram, M., & Owliaie, H. R. (2019). Prediction of soil clay minerals from some soil properties with use of feature selection algorithm and ANFIS methods. *Soil Research*, *57*(7), 788-796.

Nanda, A., Sen, S., Sharma, A. N., & Sudheer, K. P. (2020). Soil Temperature Dynamics at Hillslope Scale—Field Observation and Machine Learning-Based Approach. *Water*, *12*(3), 713.

Padarian, J., Minasny, B., & McBratney, A. B. (2020). Machine learning and soil sciences: A review aided by machine learning tools. *Soil*, *6*(1), 35-52.

Plauborg, F. (2002). Simple model for 10 cm soil temperature in different soils with short grass. *European Journal of Agronomy*, *17*(3), 173-179.

Pouladi, N., Jafarzadeh, A. A., Shahbazi, F., & Ghorbani, M. A. (2019). Design and implementation of a hybrid MLP-FFA model for soil salinity prediction. Environmental earth sciences, 78(5), 159.

Qais, M. H., Hasanien, H. M., & Alghuwainem, S. (2019). Identification of electrical parameters for three-diode photovoltaic model using analytical and sunflower optimization algorithm. *Applied Energy*, *250*, 109-117.

Qasem, S. N., Ebtehaj, I., & Riahi Madavar, H. (2017). Optimizing ANFIS for sediment transport in open channels using different evolutionary algorithms. Journal of Applied Research in Water and Wastewater, 4(1), 290-298.

Qi, J., Li, S., Li, Q., Xing, Z., Bourque, C. P. A., & Meng, F. R. (2016). A new soil-temperature module for SWAT application in regions with seasonal snow cover. *Journal of Hydrology*, *538*, 863-877.

Qi, J., Zhang, X., & Cosh, M. H. (2019). Modeling soil temperature in a temperate region: A comparison between empirical and physically based methods in SWAT. *Ecological Engineering*, *129*, 134-143.

Riahi-Madvar, H., Dehghani, M., Parmar, K. S., Nabipour, N., & Shamshirband, S. (2020). Improvements in the Explicit Estimation of Pollutant Dispersion Coefficient in Rivers by Subset Selection of Maximum Dissimilarity Hybridized With ANFIS-Firefly Algorithm (FFA). IEEE Access, 8, 60314-60337.

Samadianfard, S., Asadi, E., Jarhan, S., Kazemi, H., Kheshtgar, S., Kisi, O., ... & Manaf, A. A. (2018a). Wavelet neural networks and gene expression programming models to predict short-term soil temperature at different depths. *Soil and Tillage Research*, *175*, 37-50.

Samadianfard, S., Ghorbani, M. A., & Mohammadi, B. (2018b). Forecasting soil temperature at multiple-depth with a hybrid artificial neural network model coupled-hybrid firefly optimizer algorithm. *Information Processing in Agriculture*, *5*(4), 465-476.

Sanikhani, H., Deo, R. C., Yaseen, Z. M., Eray, O., & Kisi, O. (2018). Non-tuned data intelligent model for soil temperature estimation: A new approach. *Geoderma*, *330*, 52-64.

Seifi, A., & Soroush, F. (2020). Pan evaporation estimation and derivation of explicit optimized equations by novel hybrid meta-heuristic ANN based methods in different climates of Iran. Computers and Electronics in Agriculture, 173, 105418.

Seifi, A., Ehteram, M., & Soroush, F. (2020). Uncertainties of instantaneous influent flow predictions by intelligence models hybridized with multi-objective shark smell optimization algorithm. Journal of Hydrology, 124977.

Seifi, A., Ehteram, M., Singh, V. P., & Mosavi, A. (2020). Modeling and Uncertainty Analysis of Groundwater Level Using Six Evolutionary Optimization Algorithms Hybridized with ANFIS, SVM, and ANN. Sustainability, 12(10), 4023

Shamshirband, S., Esmaeilbeiki, F., Zarehaghi, D., Neyshabouri, M., Samadianfard, S., Ghorbani, M. A., ... & Chau, K. W. (2020). Comparative analysis of hybrid models of firefly optimization algorithm with support vector machines and multilayer perceptron for predicting soil temperature at different depths. *Engineering Applications of Computational Fluid Mechanics*, *14*(1), 939-953.

Sihag, P., Esmaeilbeiki, F., Singh, B., & Pandhiani, S. M. (2020). Model-based soil temperature estimation using climatic parameters: the case of Azerbaijan Province, Iran. *Geology, Ecology, and Landscapes*, *4*(3), 203-215.

Singh, V. K., Singh, B. P., Kisi, O., & Kushwaha, D. P. (2018). Spatial and multi-depth temporal soil temperature assessment by assimilating satellite imagery, artificial intelligence and regression based models in arid area. *Computers and electronics in agriculture*, *150*, 205-219.

Stajkowski, S., Kumar, D., Samui, P., Bonakdari, H., & Gharabaghi, B. (2020). Genetic-algorithm-optimized sequential model for water temperature prediction. Sustainability, 12(13), 5374. https://doi.org/10.3390/su12135374.

Sun, M., Zhang, X., Huo, Z., Feng, S., Huang, G., & Mao, X. (2016). Uncertainty and sensitivity assessments of an agricultural–hydrological model (RZWQM2) using the GLUE method. *Journal of hydrology*, *534*, 19-30.

Tabari, H., Hosseinzadeh Talaee, P., & Willems, P. (2015). Short-term forecasting of soil temperature using artificial neural network. *Meteorological Applications*, *22*(3), 576-585.

Talaee, P. H. (2014). Daily soil temperature modeling using neuro-fuzzy approach. *Theoretical and applied climatology*, *118*(3), 481-489.

Tayebi, H. A., Ghanei, M., Aghajani, K., & Zohrevandi, M. (2019). Modeling of reactive orange 16 dye removal from aqueous media by mesoporous silica/crosslinked polymer hybrid using RBF, MLP and GMDH neural network models. *Journal of Molecular Structure*, *1178*, 514-523.

Viola, F., Noto, L. V., Cannarozzo, M., & La Loggia, G. (2009). Daily streamflow prediction with uncertainty in ephemeral catchments using the GLUE methodology. *Physics and Chemistry of the Earth, Parts A/B/C*, *34*(10-12), 701-706.

Walczak, B., & Massart, D. L. (2000). Local modelling with radial basis function networks. *Chemometrics and Intelligent Laboratory Systems*, *50*(2), 179-198.

Xing, L., Li, L., Gong, J., Ren, C., Liu, J., & Chen, H. (2018). Daily soil temperatures predictions for various climates in United States using data-driven model. *Energy*, *160*, 430-440.

Xing, L., Li, L., Gong, J., Ren, C., Liu, J., & Chen, H. (2018). Daily soil temperatures predictions for various climates in United States using data-driven model. *Energy*, *160*, 430-440.

Yang, X. S. (2010). Firefly algorithm, stochastic test functions and design optimisation. *International journal of bio-inspired computation*, *2*(2), 78-84.

Yang, X. S. (2012, September). Flower pollination algorithm for global optimization. In *International conference on unconventional computing and natural computation* (pp. 240-249). Springer, Berlin, Heidelberg.

Zeynoddin, M., Ebtehaj, I., & Bonakdari, H. (2020). Development of a linear based stochastic model for daily soil temperature prediction: One step forward to sustainable agriculture. *Computers and Electronics in Agriculture*, *176*, 105636.

Zhang, F. B., Wang, Z. L., & Yang, M. Y. (2015). Assessing the applicability of the Taguchi design method to an interrill erosion study. *Journal of Hydrology*, *521*, 65-73.

Zhao, X., Wang, C., Su, J., & Wang, J. (2019). Research and application based on the swarm intelligence algorithm and artificial intelligence for wind farm decision system. *Renewable energy*, *134*, 681-697.

Zheng, G., Zhang, W., Zhang, W., Zhou, H., & Yang, P. (2020). Neural network and support vector machine models for the prediction of the liquefaction-induced uplift displacement of tunnels. *Underground Space*.

Zolfaghari, H., Masoompour, J., Yeganefar, M., & Akbary, M. (2016). Studying spatial and temporal changes of aridity in Iran. *Arabian Journal of Geosciences*, *9*(5), 375.

Figures

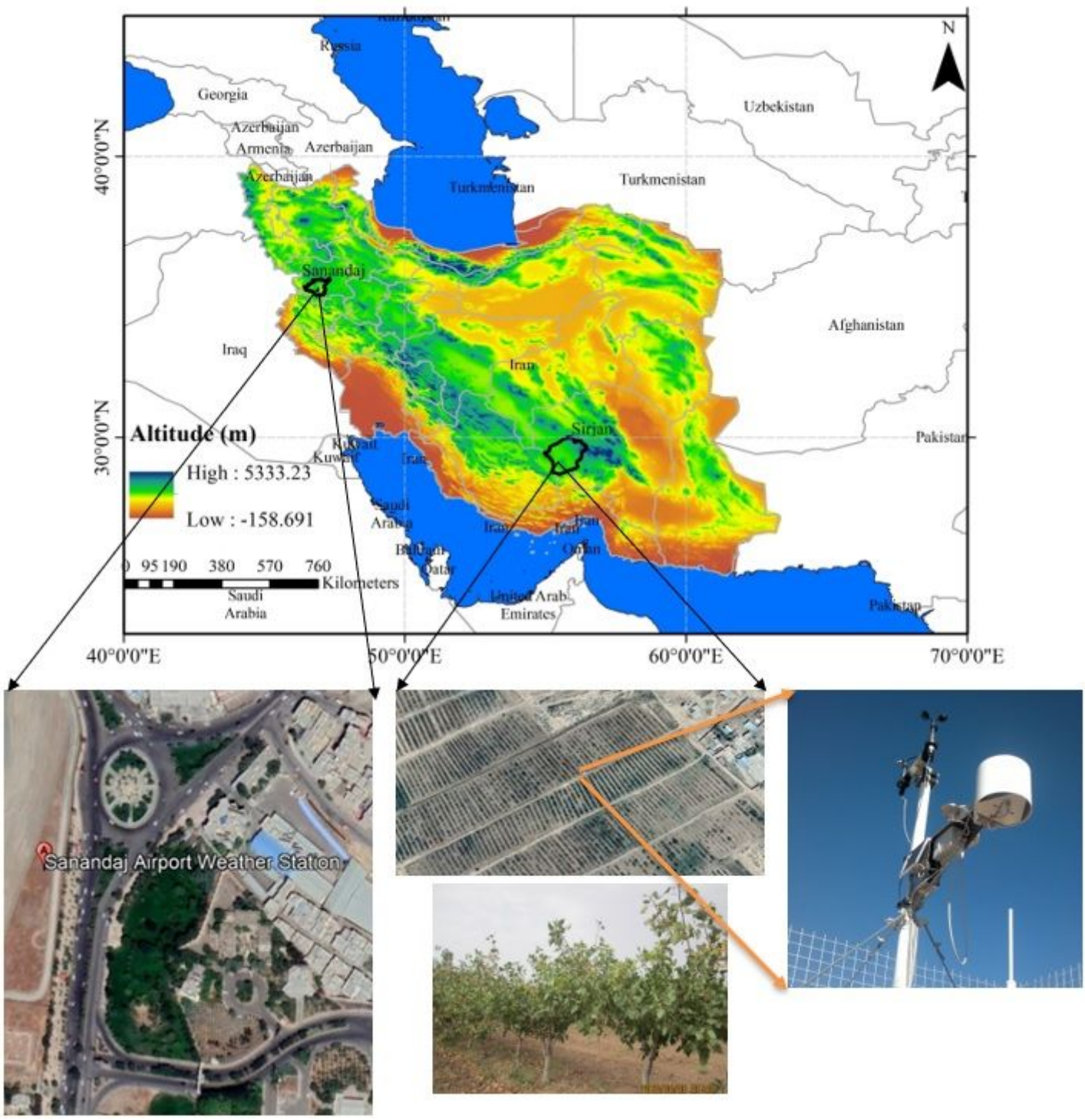

Figure 1

Location of the case study stations in Iran. Note: The designations employed and the presentation of the material on this map do not imply the expression of any opinion whatsoever on the part of Research Square concerning the legal status of any country, territory, city or area or of its authorities, or concerning the delimitation of its frontiers or boundaries. This map has been provided by the authors.

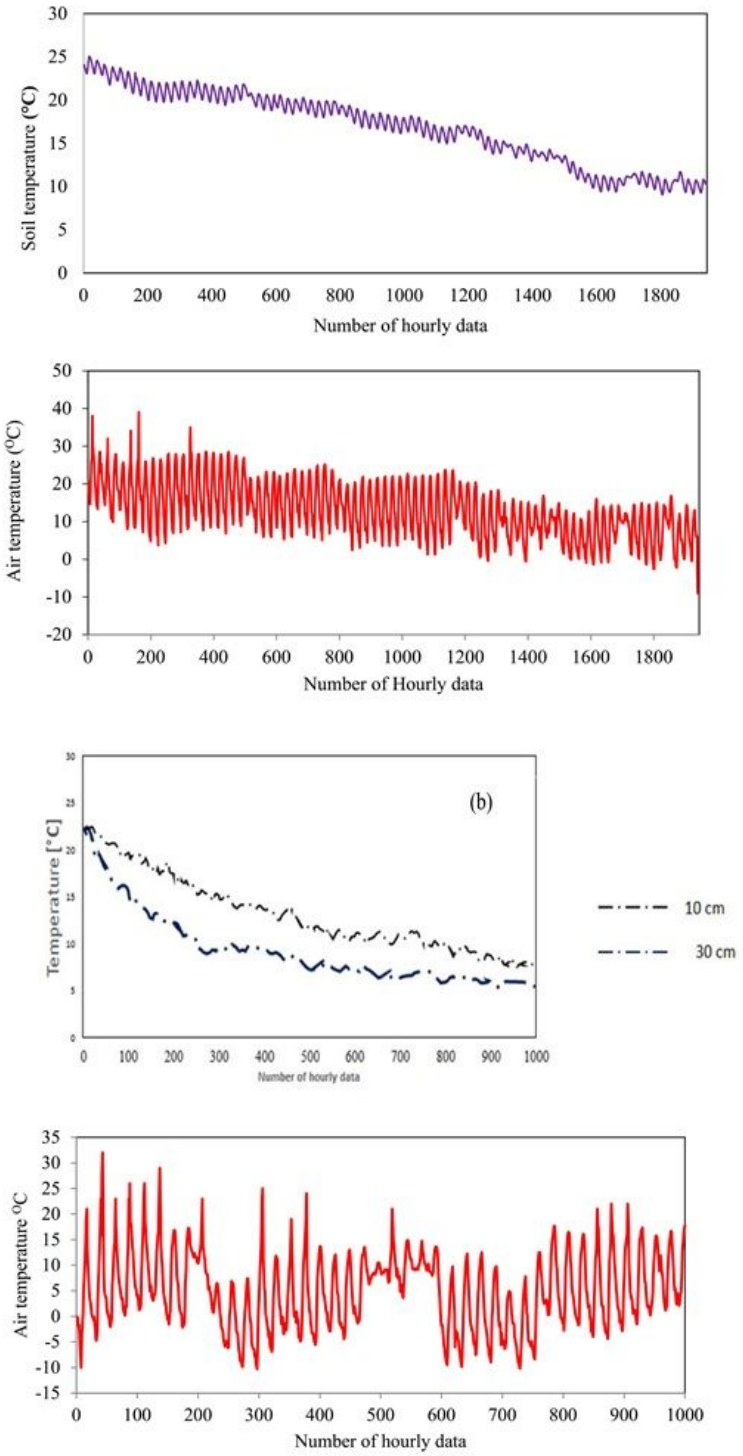

Figure 2

Time series of (1): soil temperature at (a): 5 cm depth for Sirjan and (b): 10 and 30 cm depths for Sanandaj stations, and (2) air temperature

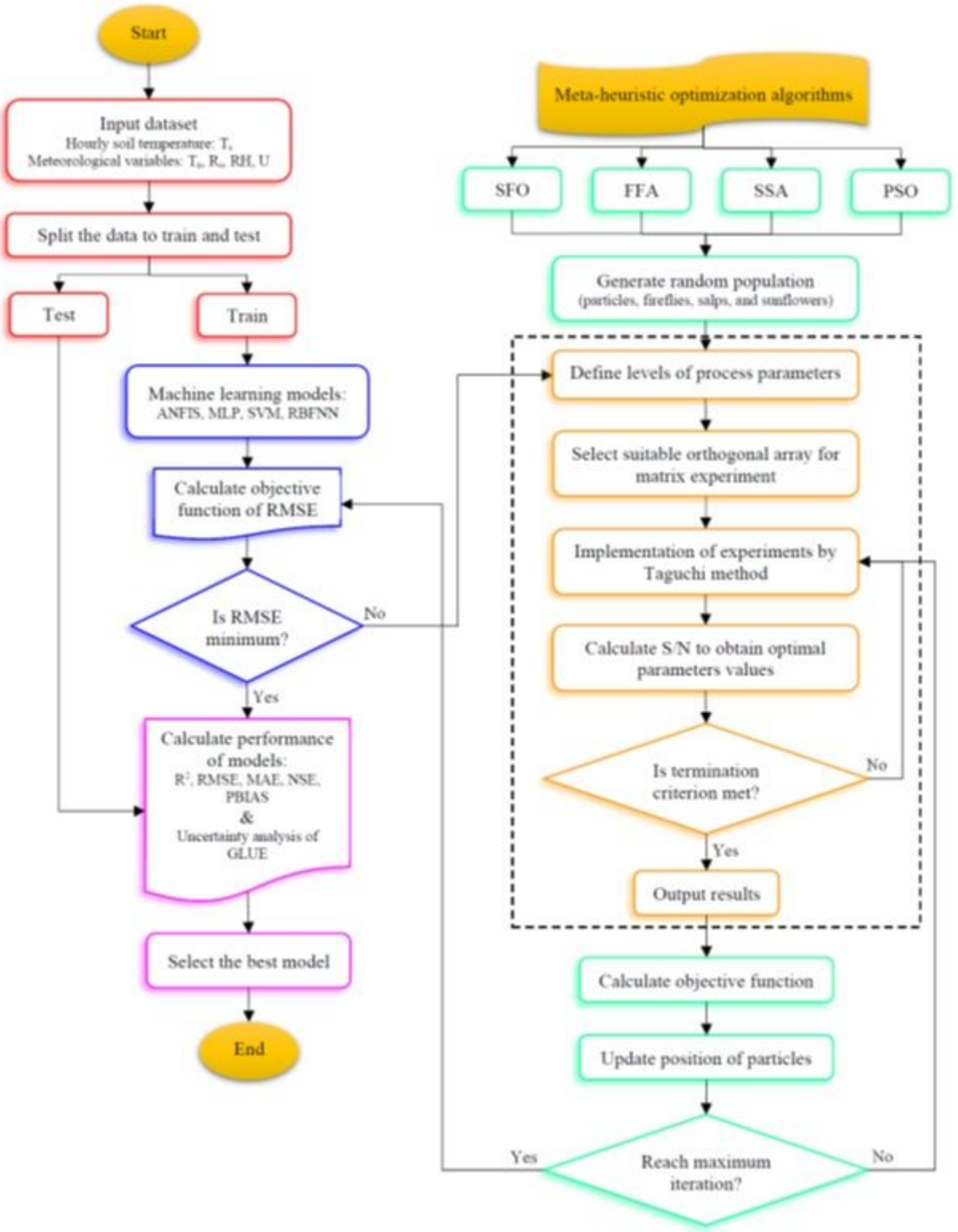

Figure 3

Framework for predicting hourly soil temperature using hybrid models.

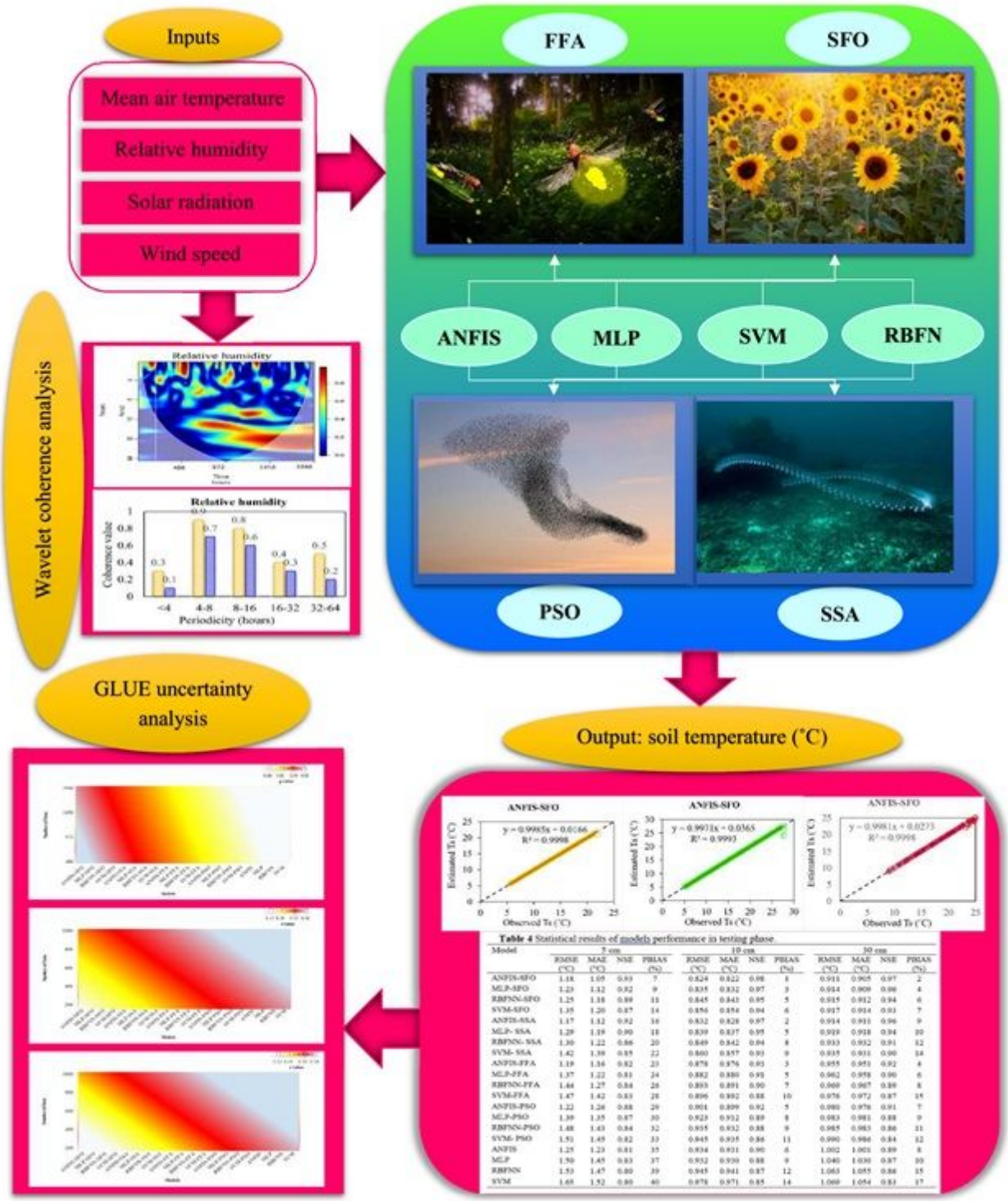

Figure 4

Schematic diagram representing the process of the study

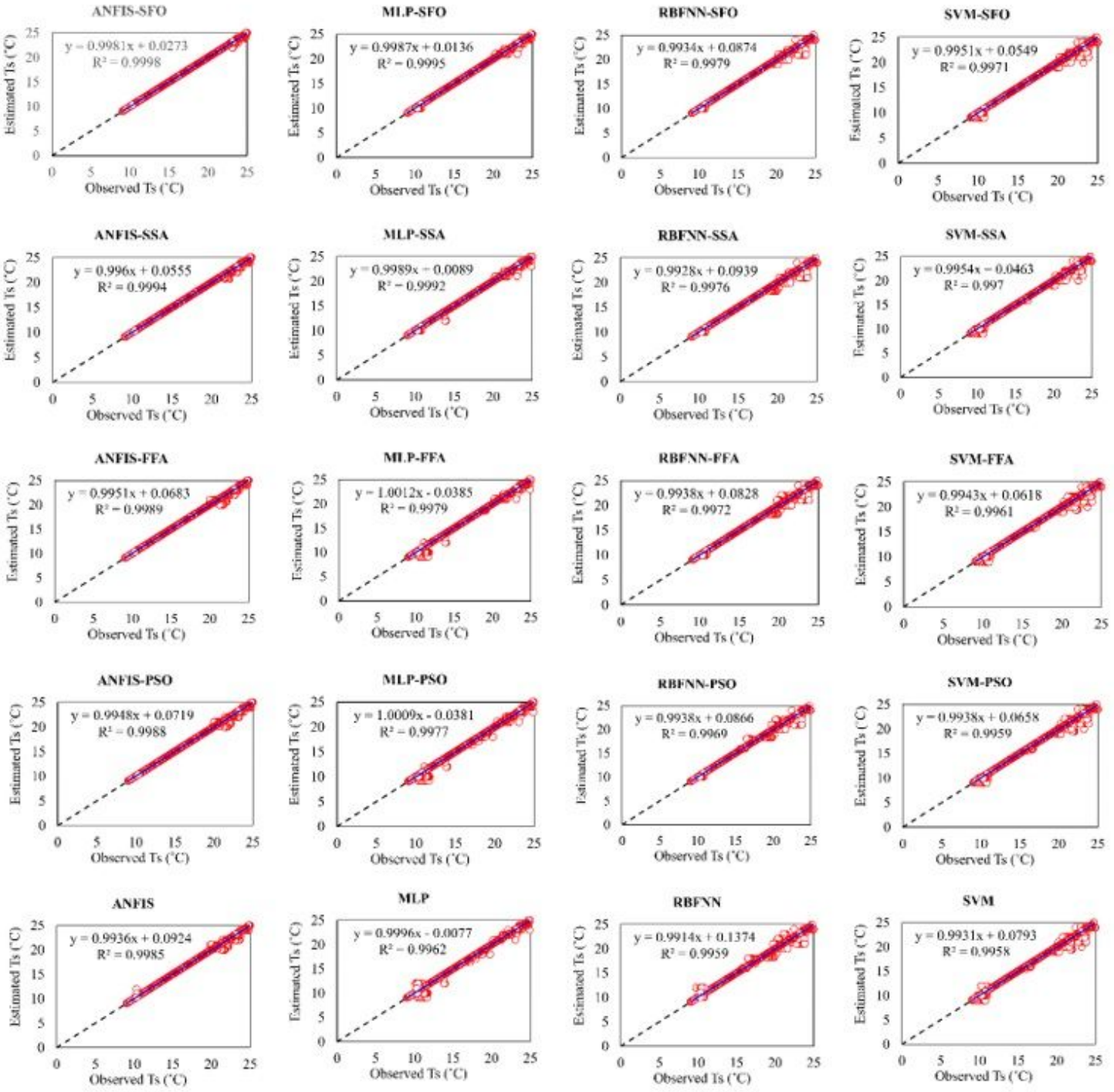

Figure 5

Soil temperatures estimated by developed hybrid and standalone models versus the measured values at 5 cm soil depth in Sirjan station

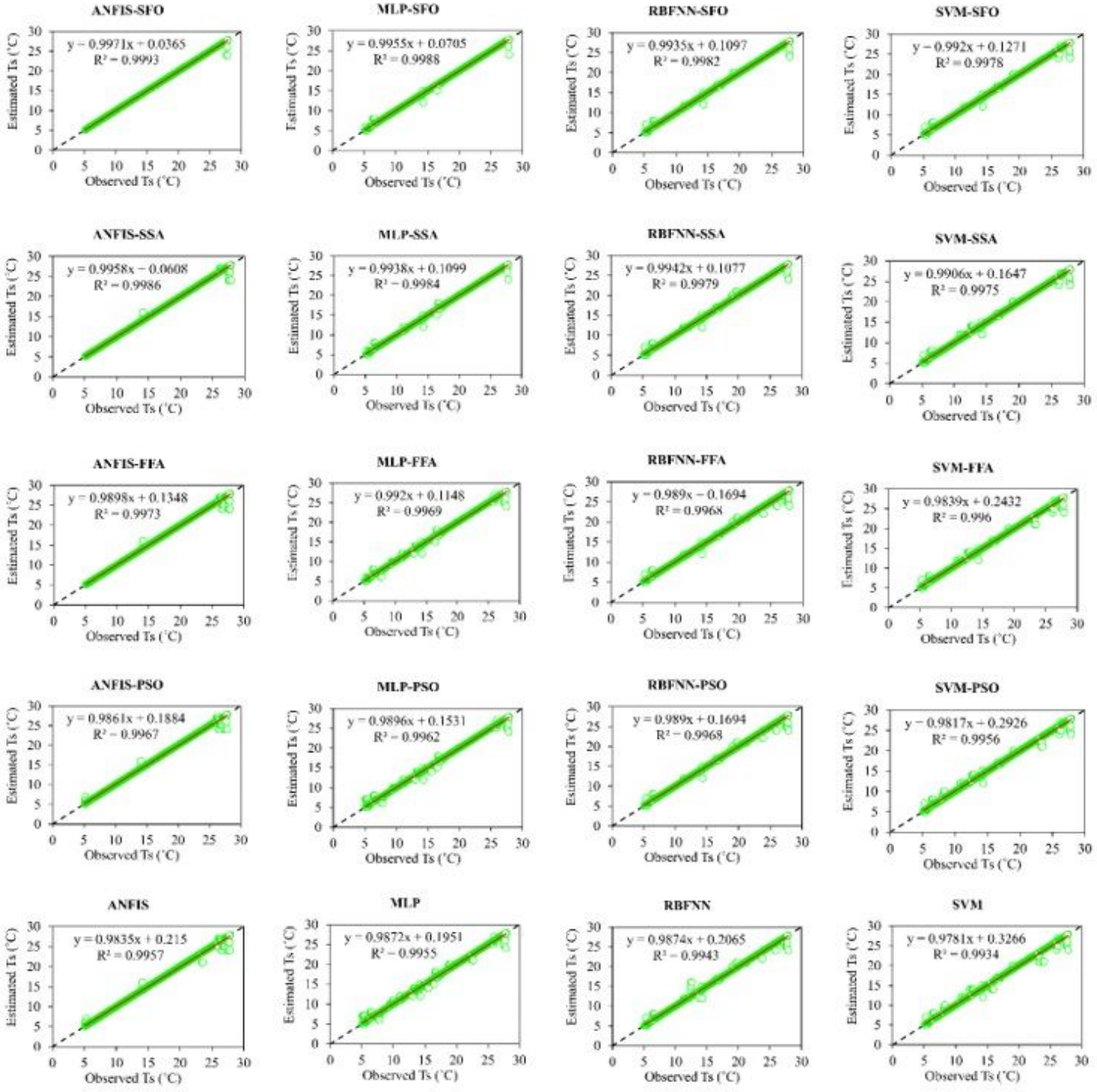

Figure 6

Soil temperatures estimated by developed hybrid and standalone models versus the measured values at 10 cm soil depth in Sanandaj station

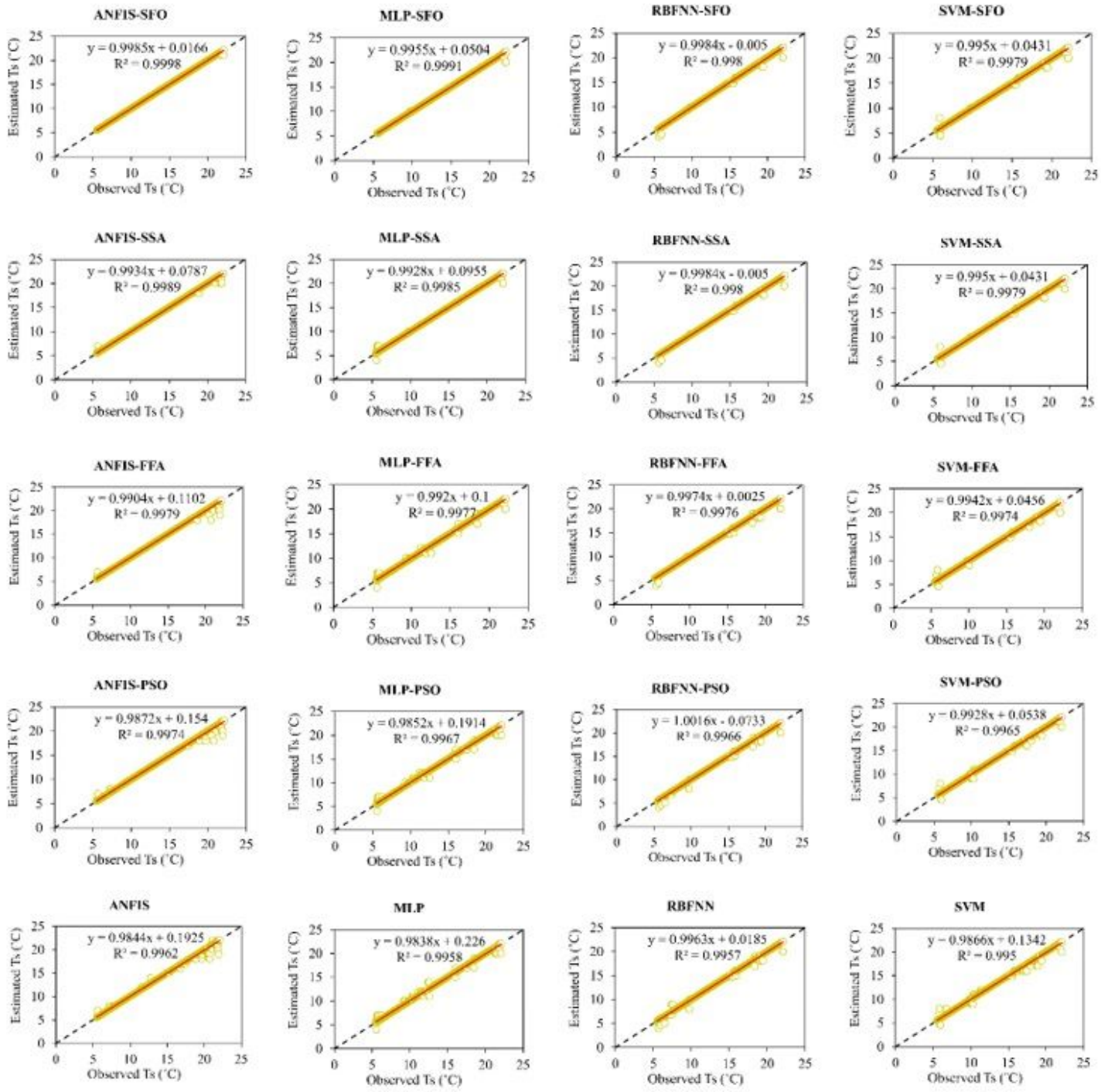

Figure 7

Soil temperatures estimated by developed hybrid and standalone models versus the measured values at 30 cm soil depth in Sanandaj station

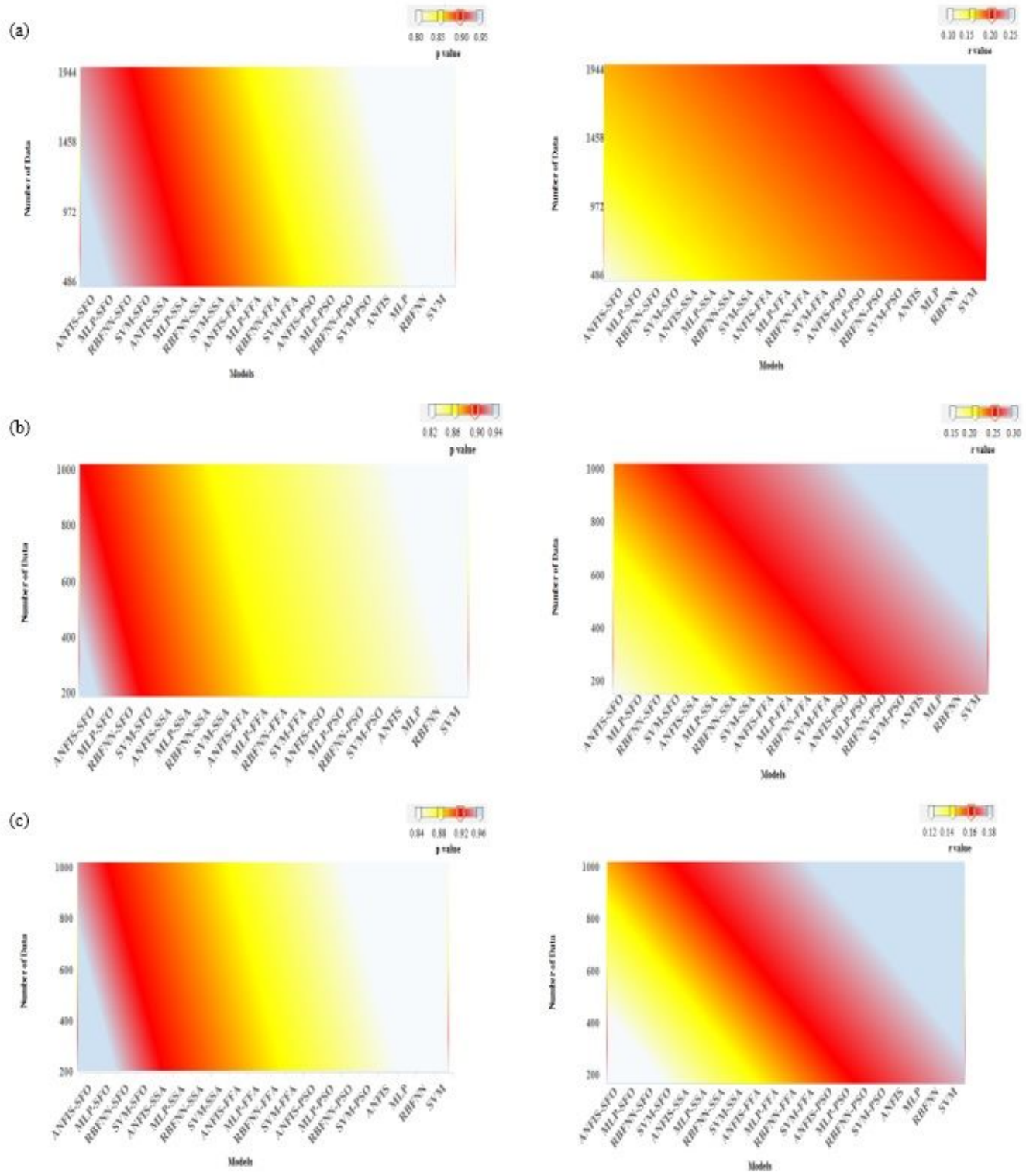

Figure 8

The uncertainty analysis based on 1: r and 2: p values at a: 5 cm, b: 10 cm and c: 30 cm soil depth in studied stations.

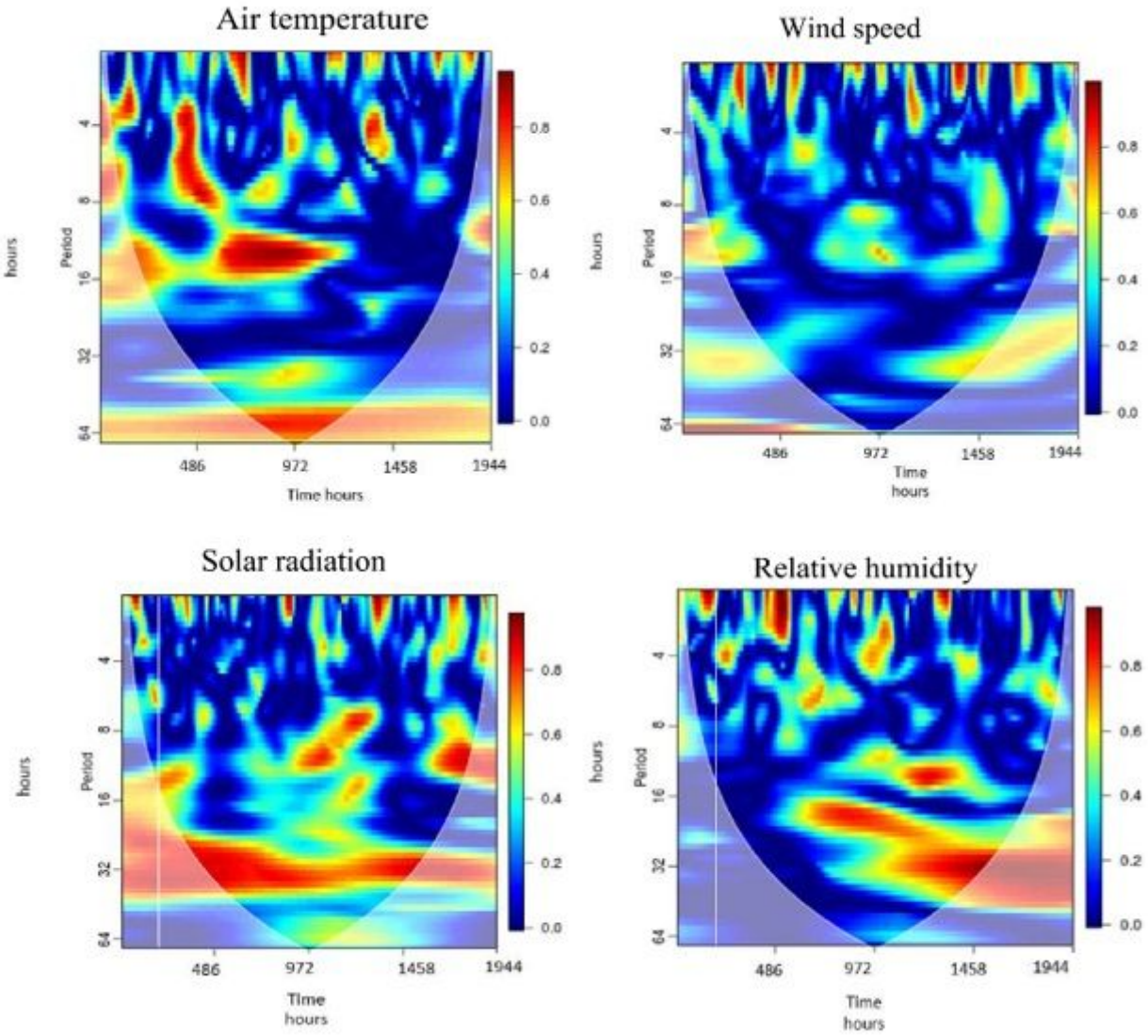

Figure 9

The coherence value for meteorological parameters in Sirjan at 5 cm soil depth

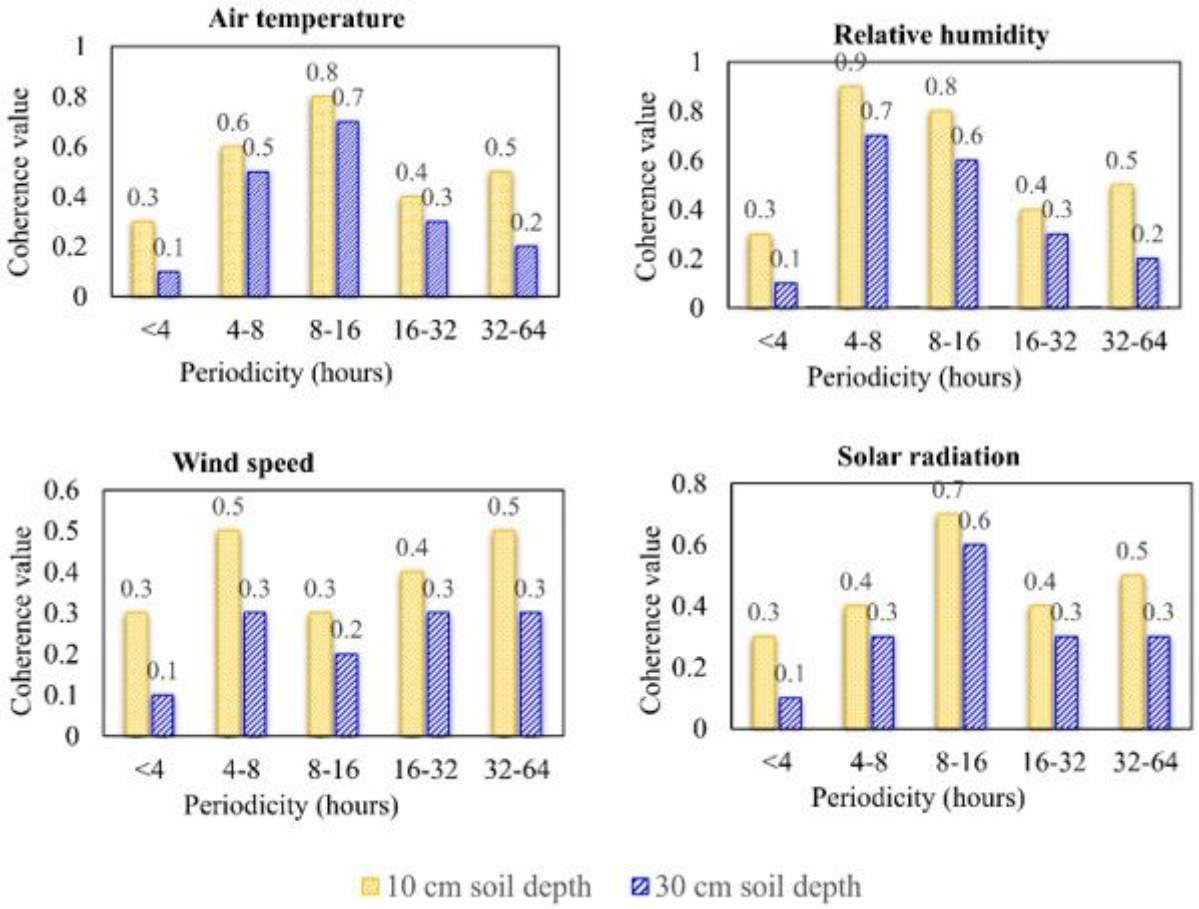

Figure 10

The coherence value for meteorological parameters in Sanandaj station at 10 and 30 cm soil depths

Supplementary Files

This is a list of supplementary files associated with this preprint. Click to download.

- Graphicalabstract.pdf